



HAL
open science

Compatibility of UN with refractory metals (V, Nb, Ta, Cr, Mo, and W): an ab initio approach to interface reactions and diffusion behavior

Huan Liu, Diogo R. Costa, Denise A. Lopes, Antoine Claisse, Luca Messina,
Pär Olsson

► To cite this version:

Huan Liu, Diogo R. Costa, Denise A. Lopes, Antoine Claisse, Luca Messina, et al.. Compatibility of UN with refractory metals (V, Nb, Ta, Cr, Mo, and W): an ab initio approach to interface reactions and diffusion behavior. *Journal of Nuclear Materials*, 2022, 560, pp.153482. cea-03697919

HAL Id: cea-03697919

<https://cea.hal.science/cea-03697919>

Submitted on 17 Jun 2022

HAL is a multi-disciplinary open access archive for the deposit and dissemination of scientific research documents, whether they are published or not. The documents may come from teaching and research institutions in France or abroad, or from public or private research centers.

L'archive ouverte pluridisciplinaire **HAL**, est destinée au dépôt et à la diffusion de documents scientifiques de niveau recherche, publiés ou non, émanant des établissements d'enseignement et de recherche français ou étrangers, des laboratoires publics ou privés.

Compatibility of UN with refractory metals (V, Nb, Ta, Cr, Mo and W): an *ab initio* approach to interface reactions and diffusion behavior

Huan Liu,¹ Diogo R. Costa,¹ Denise A. Lopes,^{1,2} Antoine Claisse,² Luca Messina,³ and Pär Olsson^{1,*}

¹*KTH Royal Institute of Technology, 10691 Stockholm, Sweden*

²*Westinghouse Electric Sweden, SE-72163, Västerås, Sweden*

³*CEA, DEs, IRESNE, DEC, Cadarache F-13108 Saint-Paul-Lez-Durance, France*

Uranium mononitride (UN)-uranium dioxide (UO₂) composites are being considered as an innovative advanced technology fuel option for light water reactors, where an optimal balance between the chemical advantages of UO₂ and the thermal and neutronic properties of UN is struck. However, the effect and extent of chemical interactions between UN and UO₂ during sintering and operation are still open issues of importance. A possibility to avoid these interactions is to protect the UN phase before sintering the UN-UO₂ composites by encapsulating the UN. This protective material must have a high melting point, high thermal conductivity, and reasonably low neutron cross-section. Among many candidates, the use of refractory metals is a promising option. In this study, density functional theory calculations (DFT) were performed to study the interactions and kinetics at the UN-X interfaces respectively (X=V, Nb, Ta, Cr, Mo, and W). The diffusion behaviors in UN and in the metal were studied using the self-consistent mean field (SCMF) theory. Generally, the diffusion of metal atoms in UN is slow compared to the diffusion of N atoms in the metals. Furthermore, the DFT calculations predict that Ta and V may react with UN to form UTaN₂ and V₈N at the UN-X interfaces, respectively. In some cases, the formation of these phases also promotes the formation of point defects in the UN and metal phases. The interaction between W and Mo with the UN phase is largely prohibited. According to this work, Mo and W can be regarded as highly promising candidate materials for fabrication of stable UN-UO₂ composite fuel.

I. INTRODUCTION

Uranium nitride (UN) has been considered one of the most promising fuels to substitute UO₂ in light water reactors (LWRs), mainly due to its higher uranium density, thermal conductivity, and similar melting point in comparison with UO₂ [1]. Nevertheless, its low oxidation resistance when in contact with the coolant water is a major drawback of using UN in LWR [2]. In an eventual accident scenario, the UN fuel would readily react exothermically with e.g. water and cause fuel pellet oxidation and pulverization [3–5]. The reaction is fortunately slow enough to prevent neighboring rods from failing.

Composite fuels have been proposed to overcome the low oxidation resistance of UN. In such concepts, some materials have been added to UN to act as a barrier against the oxidation: USi_x, CrN and AlN [6], ZrN [7], U₃Si₂ [8, 9], and UO₂ [10–13]. Among these materials, UO₂ is considered a particularly promising candidate since it is already used in LWRs and has a good oxidation resistance against water. However,

previous studies have proposed or identified a formation of a sesquinitride phase, α -U₂N₃, during the UN-UO₂ composite fabrication [10–12]. Recently, Costa et al. [13] proposed a mechanism for the formation of this detrimental α -U₂N₃ phase, as well as identified that its growth during fabrication can be minimized by tuning the spark plasma sintering parameters. However, in operating conditions (> 1000 K), the UN and UO₂ would interact anyway and should form the undesired U₂N₃ phase. Therefore, an optimization of such composite must be performed to avoid this interaction not only during fabrication but also in operating conditions.

An option to avoid the interaction between the UN and UO₂ is to protect the nitride phase by encapsulating it before sintering the composite. The material used to protect the UN must have a high melting point, high thermal conductivity and reasonably low neutron cross-section. Among many possible candidates, refractory metals have great potential.

Studies dating back to the early 1960s have experimentally investigated the interactions between refractory metals (W, Mo, Ni, and Ta) and UO₂ in the quest for utilization of the refractory-metal-clad nuclear fuel elements as thermionic cathodes [14]. In their studies, no reactions were observed between

* Corresponding author; polsson@kth.se

UO₂ and any of the metals at 1200 °C. At 1800 °C and 2000 °C, tungsten was found not to react with the UO₂, but niobium, tantalum, and molybdenum gave evidence of grain-boundary attack by some fission products emanating from the UO₂.

Cermets such as Mo/UO₂, W/UO₂, Mo/UN, and W/UN are being considered as fuel elements of the nuclear thermal propulsion (NTP) for manned missions to the outer planets [15]. At the W/UO₂ boundary, an anomalous ternary phase U_{0.1}WO₃ with space group Pm-3m (221) was observed at 1600 °C due to the availability of oxygen vacancies from the UO₂ reduction while sintering in vacuum. At 1850 °C, no evidence shows the formation of the ternary phase. It was also reported in this experiment that uranium diffused approximately 10 nm into the tungsten matrix and the presence of free uranium was explained in terms of oxygen vacancy generation due to processing in vacuum. No evidence of chemical incompatibility between UN and the metals (Mo and W) was observed, provided that nitrogen was present over the cermet at temperatures above 1500 °C. When nitrogen was not present, evidence of UN decomposition and liquid-phase sintering was found. This decomposition and liquid-phase sintering appeared to be more severe in Mo/UN than in W/UN cermet [16].

In this study, we present density functional theory (DFT) calculations of the interface interactions and diffusion behaviors at the UN-X interfaces (X=V, Nb, Ta, Cr, Mo, W). The findings may guide future experimental works to overcome the interaction of UN fuels in UO₂ matrices.

II. THEORY AND METHODOLOGY

A. Interface reactions

The simulations in this work have been carried out within the framework of density functional theory (DFT) as implemented in the Vienna Ab initio Simulation Package (VASP) [17–20]. The chemical elements were modeled using the Projector Augmented Wave potentials [21] provided with the GGA-PBE [22] electron exchange correlation. The potentials were taken from VASP database, treating 14 and 5 electrons as valence for uranium and nitrogen respectively. The number of valence electrons of the refractory metals is fixed to 11 for V, Nb, and Ta, and 12 for Cr, Mo, and W, respectively. To better describe the strongly correlated f-electrons of uranium

atoms, the rotationally invariant implementation of the Hubbard-*U* correction introduced by Liechtenstein *et al.* [23] was adopted. The on-site Coulomb interaction parameter *U* and the exchange parameter *J* were set to 2.0 and 0.1 eV respectively, following optimisations in previous work [24]. A plane wave cut-off energy of 600 eV was used for all the calculations. The fractional electron occupancies were treated with the method of Methfessel-Paxton with a smearing width of 0.1 eV. The Brillouin zone (BZ) was sampled with Monkhorst-Pack (MP) meshes [25] and the k-point density was chosen to be sufficiently large for energy convergence, i.e. 4×4×4 for supercells containing 64 atoms and 2×2×2 for supercells containing 128 atoms. The convergence criterion for the geometry and ionic position optimizations were set to 0.01 eV/Å.

Rock-salt structured UN with antiferromagnetic (AFM) ordering was investigated in this work. An orthorhombic structure with lattice parameter: *a* = 5.03 Å, *b* = 4.97 Å, and *c* = 4.90 Å, which corresponds to the energetic ground state reported in [24], was chosen as the initial structure. The refractory metals V, Nb, Ta, Cr, Mo, and W, were modeled as bcc structures for the reference calculations. The structural symmetry and Wyckoff positions of the possible interaction product compounds were chosen from the Materials Project [26]. Unit cell sizes of up to four formula units of these phases were fully relaxed for computing the formation enthalpies which were further applied to the calculations of the possible interface reaction enthalpies. The point-defect formation energies in UN were calculated using a 64-atom supercell, which contains 32 uranium atoms, while the point-defects formation energies in the metals were calculated using a 128-atom supercell.

To model the fuel/metal interactions, we initially calculated the UN/metal reaction enthalpies. This is related to the probability of forming different binary and ternary phases at the interface. The reaction enthalpies, ΔH_r , were calculated using:

$$\Delta H_r = \frac{1}{N_r} \left(\sum_i^p c_i \Delta H_f^i - \sum_j^r c_j \Delta H_f^j \right) \quad (1)$$

where *i* and *j* represent the reactants and products respectively. ΔH_f are the formation enthalpy (per formula unit) and *c* the reaction coefficient of the products or reactants. The sums take into account all products, *p*, and all reactants, *r*, and *N_r* is the total number of atoms participating in the reaction.

A reaction with a more negative ΔH_r is more likely to occur.

The fuel/metal interaction mechanisms were further evaluated by calculating the formation energies of point defects in UN, and in the metals. The defect formation energies, ΔE_f^D , were calculated as follows:

$$\Delta E_f^D = E_{\text{tot}}^D - E_{\text{tot}}^0 - \sum_{i=1}^N \Delta N_i^D (\mu_i^0 + \Delta \mu_i) \quad (2)$$

where E_{tot}^0 and E_{tot}^D are the total energies of the supercell without and with a defect, respectively, and μ_i^0 is the chemical potential of element i . ΔN_i^D is the number of atoms of type i added ($\Delta N_i^D > 0$) or removed ($\Delta N_i^D < 0$) from the perfect supercell to create the defect, and the sum takes account of all added and removed species. $\Delta \mu_i$ is the change in the chemical potential of element i resulting from an N -phase equilibrium, which can be calculated by solving the set of linear equations:

$$\Delta H_{f,k} = \sum_{i=1}^N c_{ik} \Delta \mu_i \quad (3)$$

where the $\Delta H_{f,k}$ is the formation enthalpy of the phase k , and c_{ik} is the mole fraction of element i in phase k . From Eq. 3 it is evident that to determine the $\Delta \mu_i$, the number of phases k and elements (components) i should be equal, coming from the fact that, at constant temperature and pressure, a stable state in a ternary phase system is composed of three phases. In our case, we initially consider UN and one of the metals to be in equilibrium (in contact), hence two phases are already determined, yet as there are three components, a third phase should be considered, i.e. the possible interface phases. In the case of the UN/W system, the third-phase can be WN, W_2N_3 , or WN_2 . These different third phases modify the chemical potentials of the species and therefore the formation energies.

The point defects in UN studied in this work include uranium vacancies, nitrogen vacancies, nitrogen interstitials, as well as the metal atom substitution on uranium and nitrogen sublattices respectively. The Schottky defect relaxed to the combination of a vacancy and a substitution during the ion position optimization was thus not considered in this work. Point defects in the metal bulk include vacancies, uranium and nitrogen substitutions, as well as nitrogen

at octahedral and tetrahedral interstitial positions, respectively.

The chemical potentials, μ_i^0 , of N, U, and the metals (V, Nb, Ta, Cr, Mo, and W), were chosen as the single-atom energies of nitrogen gas, α -uranium and the bcc refractory metals, respectively. It has been shown that the properties of α -U are best represented by using only GGA [27], i.e., $U = J = 0$ eV, while the lowest U value that best represent UN properties is $U = 2.0$ eV [24]. However, the applications of different Hubbard- U values result in inconsistent energy states of α -U, UN and other possible ternary phases, and thus makes these phases incomparable. Therefore, the methodology that predicts formation enthalpies by mixing GGA and GGA+ U results proposed by Jain et al. [28] was applied, where the experimentally reported formation energy of U_2N_3 [29] was used for correction.

B. Diffusion behaviors

Diffusion behaviors of impurities in UN and the metal bulk systems were investigated by computing the solute tracer diffusion coefficients, which were derived from the Onsager transport coefficients. The latter were calculated within the framework of the self-consistent mean field (SCMF) theory [30], as implemented in the KineCluE code [31]. In this model, the transport coefficients are obtained by introducing a non-equilibrium distribution function in a system characterized by a small deviation from thermodynamic equilibrium represented by chemical potential gradients (CPG) acting on defects and solutes. The transport coefficients L_{ij} reflecting the kinetic response of the system to CPG can be obtained from the Onsager relation:

$$J_i = - \sum_j L_{ij} \frac{\nabla \mu_j}{k_B T}, \quad (4)$$

where J_i denotes the atomic flux of species or defect i and $\nabla \mu_j$ the CPG of each species or defect j . More detailed explanations of this method is found in [30–32]. k_B is the Boltzmann constant and T is the temperature.

The key-input parameters for the SCMF theory are the atomic jump frequencies in the local atomic environment around the solute. In the framework of transition state theory, the jump frequency ω_{ij} for a single point defect (substitution, interstitial, or va-

cancy) moving from site i to site j is defined as:

$$\omega_{ij} = -v_{ij} \exp\left(-\frac{E_m^{ij}}{k_B T}\right) \quad (5)$$

The attempt frequency v_{ij} is related to the lattice vibrational modes, whereas the migration barriers E_m^{ij} depend on the type of moving defects and the local atomic environment. In this work, the attempt frequencies and migration energies were obtained from DFT calculations.

The set of jump frequencies ω_{ij} that needs to be calculated depends on the kinetic interaction range R_{kin} which is the maximum extension of the diffusion trajectories included in the model. The transport coefficients converge with increasing R_{kin} to an asymptotic value [31]. Previous convergence study on the simple vacancy-exchange mechanisms [31] proves that the coefficients are well converged at $R_{\text{kin}} = 4a_0$ (a_0 is the lattice parameter). Therefore, we set the kinetic range to $4a_0$. The computational load can also be reduced by setting a smaller thermodynamic range R_{th} (smaller than R_{kin}), which depends on the strength of the thermodynamic interaction between defects and solute. The binding energies of solute-defect pairs whose distance is beyond R_{th} are regarded as negligible. Here we set the thermodynamic radius R_{th} to the first nearest-neighbor (1NN) distance ($\sqrt{2}a_0$). The most important 1NN migration barriers are calculated directly using DFT and migration barriers between R_{th} and R_{kin} are obtained via the kinetically resolved activation (KRA) barrier approximation:

$$E_m^{ij} = Q + \frac{E_b^i - E_b^j}{2} \quad (6)$$

Q is a reference activation energy chosen here as the bulk vacancy migration barrier for which the vacancy is far away from the solute. E_b^i and E_b^j represent the binding energies of the initial and final configurations, respectively.

The solute-defect binding energies E_b and migration energies E_m were obtained from DFT calculations. The metallic impurities X (X = V, Nb, Ta, Cr, Mo and W) are shown to be stable substitutionally on the uranium sublattices in UN. The detailed results are presented in the supplementary materials. Therefore, the uranium vacancy-assisted migration mechanisms of X were considered as dominating in this work. The KineCluE code expands the Onsager matrix in terms of cluster contributions [31]. For vacancy-assisted diffusion of a substitutional solute, there are two ‘‘clusters’’: a mono-vacancy and a

vacancy-solute pair, given that an isolated substitutional solute is immobile. Therefore, in order to calculate the diffusion coefficients of the metal atoms in UN, two types of the migration barriers E_m^S and E_m^O were calculated, where E_m^S is the migration barriers for solutes exchanging positions with vacancies, E_m^O the migration barriers for vacancies exchanging positions with the host atoms. Considering that AFM structured UN has two different spin layers: spin up and spin down, there are two different U sublattices. Therefore, the solute or host atom (U atom) can exchange positions with the vacancy either in the same spin layer (marked as S) or in the opposite layer (marked as O), as shown in Fig.1(a).

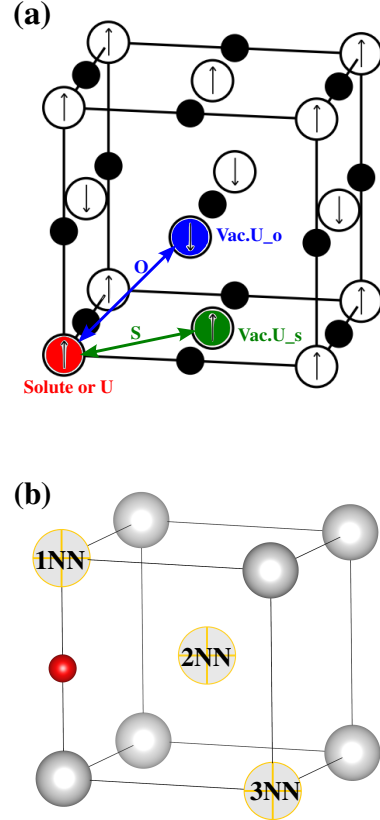


FIG. 1. (a) U vacancy-assisted jump mechanisms in UN rock-salt crystal structure with antiferromagnetic order. Uranium atoms are white while nitrogen atoms are black. The red atom represents the tracer (solute or U atom), the vacancy at the same and the opposite spin layer with the tracer are marked in green and blue respectively. (b) Atomic configurations for bcc sites of the vacancy (marked with yellow crosses) in the neighborhood of a nitrogen atom (red) at an octahedral interstitial site.

In the bulk of V, Nb, Ta, Cr, Mo and W, the solubility of N on the octahedral positions is significant and the direct interstitial migration of N from the stable octahedral position passing through the tetrahedral saddle point was thus considered. The migration of U in these metals was not considered in this work because the solubility of U in the refractory metals is exceedingly low. Here, we firstly approximate that the possible correlation effects between N interstitials and vacancies or other species are negligible and thus N atoms diffuse independently in the metal.

The DFT calculations of solute-defect binding energies E_b and migration energies E_m in UN were based on the 216-atom supercells containing 108 uranium atoms, and for the metals they were based on the 128-atom supercells, in order to avoid the self-interaction effects. The atomic positions were fully relaxed until the total energy was converged to 0.1 meV/atom and the cell shape and volume were constrained. Migration barriers were calculated using the climbing image nudged elastic band (NEB) method [33, 34] with three intermediate images. The binding energy can be calculated using the following equation:

$$E_b = E_{\text{tot}}^{\text{vac}} + E_{\text{tot}}^{\text{solute}} - E_{\text{tot}}^{\text{vac+solute}} - E_{\text{tot}}^0 \quad (7)$$

The terms in Eq. 7 are in turn the total energy of the supercell with a single vacancy, a single solute, a vacancy-solute pair, and the perfect supercell. Positive binding energies stand for attraction between the two defects, and negative binding energies stand for repulsion.

The attempt frequencies ν_{ij} of a given migration event was derived from the vibrational frequencies of the initial (I) and saddle-point (S) configurations in the framework of the harmonic transition state theory [35]:

$$\nu = \frac{\prod_{k=1}^{3N-3} \nu_k^{\text{I}}}{\prod_{k=1}^{3N-4} \nu_k^{\text{S}}} \quad (8)$$

where N is the number of atoms (216 in UN and 128 in the metals), and the index k scans through the degrees of freedom of the system. One degree of freedom is missing in the saddle-point configurations, as it corresponds to the mode for the motion of the jumping atom in the saddle-point direction, which has to be constrained. The vibrational frequencies

were computed by means of DFT frozen-phonon calculations [36] with the code Phonopy [37]. The force convergence criterion for the calculation was set to 10^{-6} eV/Å, and the total energy was relaxed until the energy difference is smaller than 10^{-8} eV. The other computational details were as same as for the NEB calculations.

Note that the defect concentrations are needed in order to compute diffusion coefficients for defect-assisted diffusion mechanisms. Metal diffusion in UN follows a vacancy-assisted mechanism. Therefore, the equilibrium concentration of uranium vacancies in UN must be known. Following the Boltzmann statistics in the dilute limit, the uranium-vacancy concentration (per atomic site) is given as:

$$C_V^{\text{eq}} = \exp\left(-\frac{G_V^{\text{f}}}{k_B T}\right) \quad (9)$$

where T is the temperature, k_B the Boltzmann constant, and G_V^{f} the uranium vacancy formation energy.

The Onsager matrix approach allows for the analysis of flux coupling between different species (vacancies V and solutes S). For the diffusion of solutes (V, Nb, Ta, Cr, Mo, or W) in UN, the flux coupling between solutes and uranium vacancies can be analyzed by computing the drag ratio $G = L_{VS}^{\text{vac}}/L_{SS}^{\text{vac}}$ and the partial diffusion coefficients (PDC) ratio which is given as [32]:

$$D_{\text{pd}} = \frac{(1 - C_S)L_{\text{BV}}^{\text{vac}}}{C_S L_{\text{AV}}^{\text{vac}}} \quad (10)$$

where $L_{\text{AV}}^{\text{vac}} = -L_{\text{VV}}^{\text{vac}} - L_{\text{VB}}^{\text{vac}}$, A and B represent the host and foreign atom, respectively. C_S is solute concentration which is fixed to 0.1 for all cases, for simplicity. In the absence of attractive interactions between defect and solute, the atomic flux is opposed to the vacancy flux, because the vacancy moves by exchanging with either solute or host atoms. However, when attractive solute-defect interactions are present, the vacancy may remain in proximity of the solute and produce consecutive solute jumps in the same direction: this is usually referred to as vacancy drag. The PDC ratio describes the relative diffusion rate of the solute with respect to matrix atoms, which determines the solute segregation or depletion tendency at defect sinks (e.g. dislocation lines, grain boundaries, free surfaces, and so on). Vacancy drag leads to solute enrichment at sinks, in which case the PDC ratio D_{pd} is negative. In the absence of vacancy drag, two regimes are possible: when $0 < D_{\text{pd}} < 1$, solutes diffuse slower than host atoms, and enrichment at sinks

TABLE I. UN/metal reaction enthalpies, ΔH_r , in eV/atom, where metals are V, Nb, Ta, Cr, Mo, and W. The reactions with the highest and lowest reaction enthalpies are marked with bold font.

Metal	Reaction	ΔH_r (eV/atom)
V	UN+8V=V ₈ N+U	0.01
Nb	2UN+Nb=UNbN ₂ +U	0.11
Ta	2UN+Ta=UTaN₂+U	-0.21
Cr	3UN+Cr=U ₂ CrN ₃ +U	0.20
Mo	UN+2Mo=Mo ₂ N+U	0.55
W	3UN+2W=W₂N₃+U	0.88

takes place; on the other hand, if $D_{pd} > 1$, solutes are faster than host atoms, and depletion thus occurs.

III. RESULTS AND DISCUSSIONS

A. Interface reactions

Using Eq. 1 we calculated the possible interface reaction enthalpies, ΔH_r , of all the configurations (UN/V, UN/Nb, UN/Ta, UN/Cr, UN/Mo, and UN/W). The reaction with the lowest reaction enthalpy of each configuration are listed in Table I, while all possible reactions and their reaction enthalpies can be found in Appendix, Table A2. The required formation energies, ΔH_f , of reactants and products are presented in Appendix, Table A1. As listed in Table I, the UN/Ta reaction having negative ΔH_r forms ternary-phase UTaN₂ and U metal (in liquid state at ordinary sintering temperature). The UN/V reaction generating V₈N and metal U has an approximately zero reaction enthalpy. This indicates that UTaN₂ and V₈N should form at the UN/Ta

and UN/V interface, respectively, driven by entropy at finite temperatures. As shown in Table A2, UTaN₂ forms at higher UN to Ta mole ratio, representing the fuel side of the fuel/metal system. This implies that UTaN₂ should exist at the UN/Ta interface near the fuel surface. Contrarily, V₈N is created at lower UN to V mole ratio, and thus exist at UN/V interface proximate to the metal surface.

On the other hand, UN/Nb, UN/Cr, UN/Mo, and UN/W interface reactions all have positive ΔH_r and the corresponding products thus have little probability to form at the interfaces, where UN/W having the highest ΔH_r is the most stable system. One should note that this DFT work simulates the reactions at 0 K. Reactions with positive 0 K ΔH_r can nevertheless be driven by entropy at finite higher temperatures or by irradiation. Therefore, different interface phases could potentially be observed at high temperature or radiation conditions. Even so, UN/W is the most stable configuration among these candidates.

However, the initial interaction is not the end of the story. The existence of the interface phases may provide a driving force for further reactions which originates from the existence of point defects in the UN and the metal. The point defect formation can thus provide a more in-depth understanding of the possible phase formation processes. The formation of any defect depends on the atomic species chemical potentials since the existence of the interfacial phases changes the chemical potentials of species i by $\Delta\mu_i$ (Eq. 2). Here, we established a three-phase equilibrium from which $\Delta\mu_i$ values can be obtained using Eq. 3. Thus, the corresponding binary and ternary vanadium nitrides, niobium nitrides, tantalum nitrides, chromium nitrides, molybdenum nitrides, and tungsten nitrides were each used to obtaining $\Delta\mu_i$ from 3-phase equilibria with UN and V, Nb, Ta, Cr, Mo and W respectively. The calculated point defect formation energies in UN and the metal using Eq. 2 are presented in Table II.

TABLE II: Defect formation energies (ΔE_f^D) in eV, in UN; and b) in X metal (X= V, Nb, Ta, Cr, Mo and W) with chemical potentials governed by the three-phase equilibrium. The negative ΔE_f^D are shown in bold font.

a) Point defect in UN						
X	Three-phase equilibrium	Vac. U	Vac. N	Inter. N	X on U	X on N
V	UN-V-V ₈ N	3.30	0.86	5.39	2.41	3.66
	UN-V-V ₂ N	3.23	0.93	5.32	2.34	3.73
	UN-V-VN	2.65	1.52	4.74	1.75	4.31
	UN-V-V ₂ N ₃	1.59	2.57	3.68	0.70	5.37

	UN-V-UVN ₂	2.87	1.29	4.96	1.98	4.09
Nb	UN-Nb-Nb ₂ N	2.95	1.22	5.04	0.93	5.73
	UN-Nb-NbN	2.45	1.71	4.55	0.43	6.22
	UN-Nb-UNbN ₂	2.72	1.44	4.82	0.70	5.95
	UN-Nb-Nb ₅ N ₆	2.17	1.99	4.26	0.15	6.51
Ta	UN-Ta-Ta ₂ N	3.07	1.10	8.13	1.12	6.01
	UN-Ta-TaN	2.66	1.50	4.76	0.72	6.41
	UN-Ta-Ta ₅ N ₆	2.39	1.77	4.49	0.45	6.68
	UN-Ta-Ta ₃ N ₅	2.00	2.16	4.10	0.06	7.07
	UN-Ta-UTaN ₂	4.43	-0.27	6.52	2.53	4.65
Cr	UN-Cr-Cr ₂ N	1.56	2.61	3.65	1.94	5.58
	UN-Cr-Cr ₃ N ₂	1.39	2.77	3.48	1.77	5.75
	UN-Cr-CrN	1.39	2.77	3.48	1.77	5.75
	UN-Cr-Cr ₃ N ₄	0.89	3.27	2.99	1.27	6.25
	UN-Cr-U ₂ CrN ₃	1.96	2.20	4.05	2.34	5.18
Mo	UN-Mo-MoN	1.22	2.94	3.31	0.85	6.26
	UN-Mo-Mo ₂ N ₃	0.83	3.33	2.62	0.45	6.65
	UN-Mo-Mo ₁₅ N ₁₆	1.17	3.00	3.26	0.79	6.32
W	UN-W-WN	0.51	3.65	2.60	0.57	8.21
	UN-W-W ₂ N ₃	1.10	3.07	3.19	1.15	7.62
	UN-W-WN ₂	0.75	3.42	2.84	0.81	7.97

b) Point defect in X metal

X	Three-phase equilibrium	Vac. X	N on X	N on octa.	N on tetra.	U on X
V	UN-V-V ₈ N	2.84	5.20	0.63	2.05	0.40
	UN-V-V ₂ N	2.84	5.12	0.55	1.97	0.48
	UN-V-VN	2.84	4.54	-0.03	1.39	1.06
	UN-V-V ₂ N ₃	2.84	3.48	-1.09	0.33	1.89
	UN-V-UVN ₂	2.84	4.76	0.19	1.61	0.83
Nb	UN-Nb-Nb ₂ N	2.41	5.09	0.10	1.54	3.80
	UN-Nb-UNbN ₂	2.41	4.87	-0.12	1.32	4.02
	UN-Nb-NbN	2.41	4.60	-0.39	1.05	4.29
	UN-Nb-Nb ₅ N ₆	2.41	4.32	-0.67	0.76	4.57
Ta	UN-Ta-Ta ₂ N	3.02	6.13	0.24	1.64	0.67
	UN-Ta-TaN	3.02	5.73	-0.16	1.24	1.73
	UN-Ta-Ta ₅ N ₆	3.02	5.46	-0.43	0.97	1.34
	UN-Ta-Ta ₃ N ₅	3.02	5.07	-0.82	0.58	2.61
	UN-Ta-UTaN ₂	3.02	7.49	1.60	3.00	-0.70

Cr	UN-Cr-Cr ₂ N	2.44	4.52	1.44	2.41	6.00
	UN-Cr-Cr ₃ N ₂	2.44	4.36	1.28	2.24	6.17
	UN-Cr-CrN	2.44	4.35	1.27	2.24	6.17
	UN-Cr-Cr ₃ N ₄	2.44	3.86	0.78	1.74	6.67
	UN-Cr-U ₂ CrN ₃	2.44	1.61	-1.47	-0.51	6.17
Mo	UN-Mo-MoN	2.61	2.80	1.64	2.31	15.80
	UN-Mo-Mo ₂ N ₃	2.61	2.41	1.25	1.92	16.19
	UN-Mo-Mo ₁₅ N ₁₆	2.61	2.75	1.58	2.25	15.86
W	UN-W-WN	3.26	5.02	1.34	2.11	4.05
	UN-W-W ₂ N ₃	3.26	5.61	1.93	2.69	3.46
	UN-W-WN ₂	3.26	5.02	1.34	2.11	4.05

According to our calculations, N is energetically favorable to incorporate in V bulk at the octahedral position, when VN or V₂N₃ exist at the UN/V interface. This implies that there is a substantial driving force towards increasing the N content in the V bulk and forming vanadium nitrides at the V side, where the most probable phase is VN due to its lowest formation energy (see Table A1). In order to form vanadium nitrides, there should be a critical number of N atoms that have left their sites, forming vacancies. Creating N vacancies in UN is energetically unfavorable and requires substantial energy, which can be available at high temperatures, or through radiation damage effects. In fact, as illustrated in Fig. 2, the N-rich phase V₂N₃ can transition to VN and then relax to hypo-stoichiometric VN_{1-x}, while releasing N atoms. The driving force for this N incorporation is stronger for V₂N₃ than for VN, because the former generates a more negative defect formation energy (-1.09 eV) than the latter (-0.03 eV). When UN and V are in equilibrium with V₈N, V₂N, or UVN₂ all defect formation energies are positive, which means that both UN and V are very stable.

N incorporation is favorable in the Nb matrix when Nb₅N₆, NbN, and UNbN₂, are considered. Similar to the situation at the UN/V interface, the N-rich phase Nb₅N₆ loses N atoms and reduces to NbN while increasing the N content at the Nb surface, and then NbN further reduces to NbN_{1-x} providing more N sources to niobium nitride formation. Also, the defect formation energy increase with the decreasing N enrichment of the interface phases weakening the driving force. The ternary phase UNbN₂ releases N atoms by decomposing into UN and Nb₂N which is

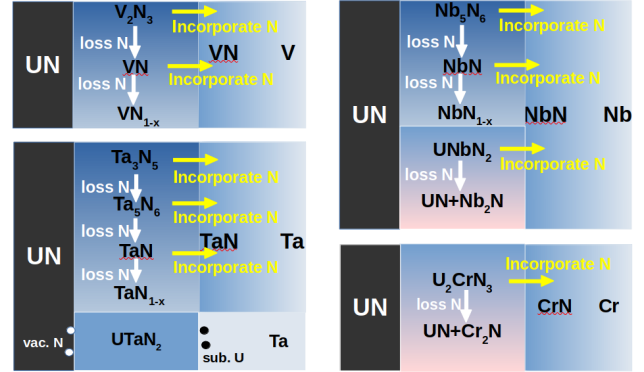


FIG. 2. Illustration of the phase transition mechanisms at the UN/Ta, UN/Nb, UN/V, and UN/Cr interfaces.

stable with respect to UN and Nb. (see Fig. 2)

The UN-Ta-UTaN₂ equilibrium promotes the formation of N vacancies in UN, thus shifting the nitrogen stoichiometry. At the same time, this equilibrium promotes the incorporation of U in Ta sublattices. The combined condition of N vacancy being favorable in UN and the U incorporation in Ta leads to the decomposition of UN, while incorporating U atoms on Ta sublattices in the Ta matrix. The removed N atoms can be trapped by the interface phase UTaN₂. UTaN₂ makes the incorporation of N in UN unfavorable. This dynamic is in agreement with the reaction enthalpies reported in Table I, which points to the possibility to reach thermodynamic equilibrium with the presence of the UTaN₂ ternary. When UN and Ta are in contact with the binary phases TaN, Ta₅N₆ or Ta₃N₅, the situation is entirely different, which is shown in Fig. 2. The presence of

these binary phases creates a driving force for N incorporation on the octahedral interstitial positions in Ta, causing the formation of tantalum nitrides. The incorporation energy diminishes with the increasing N gradient composition resulting in a weaker driving force. At the same time, these binary phases will transition from the Ta_3N to Ta_5N_6 , TaN , and finally to the hypo-stoichiometric TaN_{1-x} .

At the UN/Cr interface, binary phases are stable with UN and Cr. The existence of the ternary phase U_2CrN_3 provides a driving force to incorporate N atoms at both octahedral and tetrahedral interstitial sites in the Cr matrix, initializing the formation of chromium nitrides. This process is accompanied by decomposing U_2CrN_3 into UN and Cr_2N .

In summary, for the systems UN/V, UN/Nb, UN/Ta, and UN/Cr, the interface phases containing more than 50 at.% N promote the N incorporation in the metal matrix. Note that this does not apply to UVN_2 and UTaN_2 because of their high stabilities ($\Delta H_f = -1.43$ eV of UVN_2 and $\Delta H_f = -1.83$ eV of UTaN_2). The driving force for this incorporation is decreasing when the interface phases with less N are considered in the equilibrium. This shows the trend of the system to decrease the driving force with the N gradient composition. With this thermodynamic driving force, these phases provide N atoms for the formation of more interface phases at the metal matrix surfaces. This formation process is prevented when the N content of the interface phases is below 33.3 at.%. The existence of such phases as V_8N , V_2N , Nb_2N , and Ta_2N , causes the defect formation energies to be positive, removing the driving force for formation of the interface phases. Based on our calculations, formation of stacked phases with a N gradient are expected to be observed at UN/V, UN/Nb, UN/Ta, and UN/Cr interfaces.

For the UN/W system, when any of the three interface phases, WN , W_2N_3 , or WN_2 are present, defect formation energies in both UN and W are positive. This indicates that the UN/W system is stable and not susceptible to formation of the interface phases. The UN/Mo system behaves similarly to the UN/W system in that all the molybdenum nitrides are compatible with UN and Mo. The interface illustrations of UN/W and UN/Mo are thus not provided. These results make tungsten and molybdenum promising candidates for the UN-metal- UO_2 composite fuel.

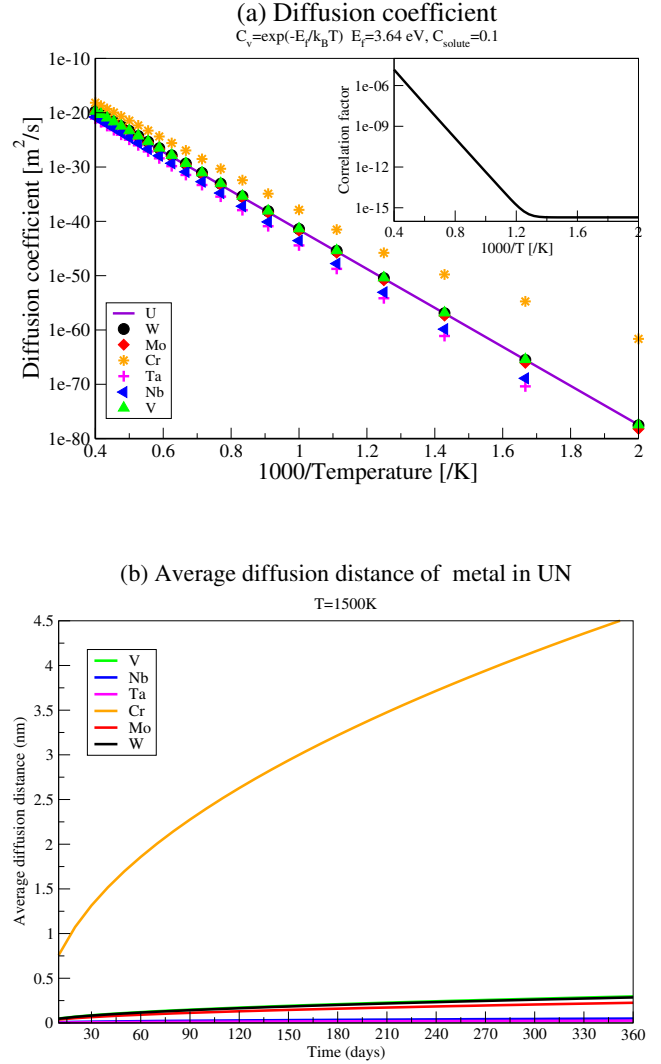


FIG. 3. (a) Diffusion coefficients of metals V, Nb, Ta, Cr, Mo, and W in UN in temperature range of 500–2500 K; (b) Average diffusion distance of metals in UN at 1500 K.

B. Diffusion behaviors in UN

The calculated diffusion coefficients of X (X= V, Nb, Ta, Cr, Mo, and W) in UN are presented in Fig. 3(a). The required parameters to compute the diffusion coefficients, including the binding and migration energies, are collected in Table III. Comparing the migration barriers E_m^{ji} and E_m^{ji} of mechanism S and O (in and out of the spin-aligned plane, respectively), one can notice that, for V and Mo, migration barriers of mechanism O are lower than that of mech-

anism S and thus mechanism O is the dominant jump mechanism. While for Nb, Ta, Cr, and W, the diffusivity is determined by mechanism S. Among these metals, Cr has the lowest migration barriers ($E_m^{j_i} = 0.73$ eV, $E_m^{j_i} = 0.77$ eV), diffusing significantly faster than the remaining metals in the entire investigated temperature range. Ta and Nb atoms diffusing at similar rates are the slowest species because of their higher migration barriers ($E_m^{j_i} = E_m^{j_i} = 4.19$ eV of Ta and $E_m^{j_i} = 3.78$ eV, $E_m^{j_i} = 3.91$ eV of Nb). The diffusion coefficients of W, Mo and V are slightly higher than those of Nb and Ta but lower than that of Cr. Fig. 3(b) shows the diffusion length scale of metal atoms in UN at 1500 K. In one year, the average diffusion distance of Ta and Nb in UN are respectively 0.03 nm and 0.05 nm. The average diffusion distance of Mo, W and V are respectively 0.23 nm, 0.29 nm, and 0.30 nm. The diffusion distance of Cr reaches 4.55 nm in one year. Nevertheless, compared to the average grain size of UN reported in [38] which is 5-30 μm , the diffusivity of these metals in UN can be considered negligible.

One can also note that, as shown in Fig. 3(a), Cr displays two different Arrhenian behaviors with a change of the slope (i.e. activation energy Q) around 800 K. The activation energy for Cr diffusion in UN below 800 K is higher than the activation energy above 800 K. The activation energy is mainly influenced by three factors: the solute migration barrier (E_m^S), the 1NN binding energy (E_b^{1NN}), and the correlation factor (CF). The correlation factor accounts for repeated exchanges between vacancy and solute (forward and backward) that do not produce a net solute displacement. CF can range from 0 to 1. The inset of Fig. 3(a) presents the correlation factor of Cr and U vacancies in UN, which clearly indicate that the CF follows an Arrhenius law above 800K while remaining constant below 800K causing the change of activation energy.

Fig. 4(a) and (b) show the flux coupling character between X (X= V, Nb, Ta, Cr, Mo, and W) and uranium vacancies, i.e. the drag ratio $G = L_{VS}/L_{SS}$ and the ratios of partial diffusion coefficients D_{pd} . Positive drag ratios indicate that the vacancy and X fluxes are in the same direction, while negative values mark fluxes in opposite directions. The PDC ratio describes the relative diffusion rate of solute with respect to matrix atoms. At temperatures above 800 K, Cr is expected to diffuse by drag of U vacancies since the drag ratio is positive. This vacancy drag enables the Cr enrichment at defect sinks ($D_{pd} < 0$,

not shown in Fig. 4(b)). For V, Nb, Ta, Mo, and W, the drag ratios are negative at the temperature higher than 800 K, these metal atoms and the uranium vacancies thus migrate in opposite directions. Although vacancy drag is absent for these metals, enrichment at sinks occurs via the inverse Kirkendall mechanism ($0 < D_{pd} < 1$) because all these metals diffuse slower than the host uranium atoms. This enrichment helps to prevent the dispersion of the impurities in UN.

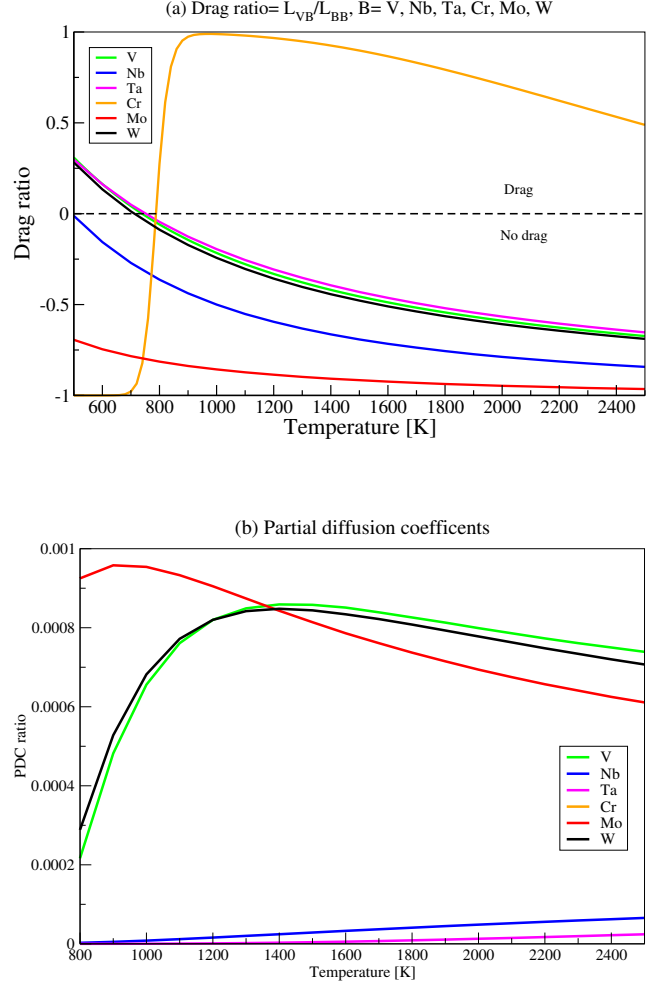


FIG. 4. (a) Solute-vacancy drag tendencies as functions of temperature; (b) Ratio of solute-to-uranium partial diffusion coefficients.

The unique curve shape of Cr-U vacancy drag ratio that switch-over from saturated -1 to near +1 and then lost with increasing temperature originates from the low migration barrier of Cr. At $T < 800$ K, mechanism S with the lowest migration barrier is the only

TABLE III. The binding energy E_b and migration energy E_m for metal diffusion in UN, in eV, where the superscript i and j correspond to the initial state and final state respectively. Mechanism S is the jump mechanism where the tracer atom is exchanging position with a vacancy in the same spin layer, while mechanism O is exchanging position with a vacancy in the opposite spin layer. Note that the migration energies listed here were all computed using DFT-NEB while the barriers of jumps beyond R_{th} were computed with the KRA method and are not listed here.

Tracer	Mechanism S				Mechanism O			
	E_b^i	E_b^j	E_m^{ij}	E_m^{ji}	E_b^i	E_b^j	E_m^{ij}	E_m^{ji}
V	0.10	0.07	2.38	2.36	0.11	-0.03	2.08	1.95
Nb	-0.13	-0.01	3.78	3.91	0.07	-0.14	4.02	3.81
Ta	0.10	0.10	4.19	4.19	0.10	-0.09	4.24	4.05
Cr	0.34	0.37	0.73	0.77	0.26	0.56	1.06	1.36
Mo	0.03	-0.02	3.06	3.01	0.02	-0.02	2.76	2.72
W	0.06	0.03	2.84	2.81	0.10	0.01	3.04	2.94
U	0.00	0.00	3.62	3.40	0.00	0.00	3.47	3.44

one mechanism active, and since this barrier is much lower than the U vacancy escape barrier (Table III), the solute-vacancy pair cannot dissociate, thus there is a super strong correlation with maximum drag effect. As T goes above 800 K, mechanism O gradually kicks in. This mechanism opens an escape route for the vacancy with a probability that, with increasing temperature, becomes comparable to that of the U vacancy sticking around. This is why the drag tendency is quickly lost as the U vacancy can escape as it pleases.

C. Diffusion behaviors in metals (V, Nb, Ta, Cr, Mo, and W)

The diffusion coefficients of nitrogen in the metal bulks are presented in Fig. 5, and the required migration barriers are listed in Table IV. Note that Table IV collects DFT calculation results which are 1NN migration barriers while the remaining ones outside of R_{th} are obtained via the KRA approximation (Eq. 6) and are not listed here. The attempt frequencies (Eq. 5) were computed with the DFT frozen-phonon method using Eq. 10. However, some of the obtained values are unreasonable. In this case, we get the attempt frequencies by fitting our computed diffusion coefficient to the experimental data and the results are reported in Table V.

According to our calculations, nitrogen diffuses faster in the metals of group VI (Cr, Mo, W) than

TABLE IV. Migration barriers E_m (in eV) of nitrogen diffusing from octahedral to octahedral interstitial sites. E_m^* is the migration barrier of the jump with a vacancy at the first-nearest neighbor (1NN) position of N.

Matrix	E_m	E_m^*
V	1.45	
Nb	1.50	
Ta	1.48	
Cr	0.98	1.48
Mo	0.70	1.66
W	0.76	1.59

in the metals of group V (V, Nb, Ta). Our calculated diffusion coefficients of Ta, Nb, V, and Cr match well with the experimental results. For the diffusion of nitrogen in W and Mo, our predicted activation energies are smaller than the experimental observations [39–42]. This indicates that interstitial migration is not the only migration mechanism of nitrogen in W and Mo. In fact, the sample applied in experimental observations contains various defects and impurities that may affect the obtained diffusion coefficient leading to a difference with respect to the theoretical calculations. To confirm this, we computed the binding energies of vacancy-nitrogen pairs in Cr, Mo, W, and Ta respectively, the results are

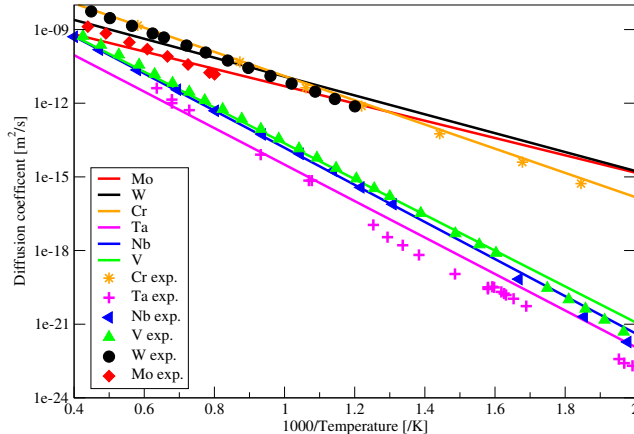


FIG. 5. Diffusion coefficient of N in metal matrices. Experiment data for Cr are reported in [39], Ta, Nb, and V in [40], W in [41], and Mo in [42]

TABLE V. Comparison of attempt frequencies (in THz) of N in metals obtained by DFT calculation and by fitting.

Matrix	DFT frozen-phonon	Fitting
V	191.00	30
Nb	*	30
Ta	25.9	5
Cr	8.49	80
Mo	1.08	1
W	2.14	5

*We were not able to calculate a reasonable attempt frequency for Nb and thus we use an experimental fitting for that element.

listed in Table VI. The configurations of the clusters are shown in Fig. 1(b). The calculated binding energies show that nitrogen atoms strongly bind to vacancies at 1NN and 2NN positions in Cr, Mo, and W but is repulsive to vacancies in Ta. Moreover, as listed in Table IV, the presence of vacancies significantly increases the migration barrier of N in Cr, Mo, and W by decreasing the diffusivity of N. This observation agrees with the results reported in Ref. [43] that proton radiation increases nitrogen solubility and decreases diffusivity in Mo. It is reasonable to speculate that N diffusivity in the metals of group V is relatively insensitive to radiation because N prefers to diffuse freely instead of binding to the vacancies. At the same time, N in the metals of group VI six

TABLE VI. Binding energies, in eV, of vacancy-nitrogen clusters in Cr, Mo, W, and Ta matrix respectively. A positive value means vacancy and nitrogen are attractive while negative stands for repulsive.

Matrix	E_b^{1NN}	E_b^{2NN}	E_b^{3NN}
Cr	1.52	0.48	
Mo	1.91	0.68	0.33
W	2.30	0.92	0.28
Ta	0.38	-0.24	

diffuses slower under radiation than in thermal conditions because the existence of vacancies coupled with the binding will increase the effective migration barrier.

IV. CONCLUSIONS

In this work, we present a detailed investigation of the interaction between UN and the refractory metals V, Nb, Ta, Cr, Mo, and W, using DFT calculations. The calculated reaction enthalpies suggest that Ta and V have relatively high propensity to react with UN, forming interface phases $UTaN_2$ and V_8N respectively. $UTaN_2$ should exist at the UN/Ta interface on the fuel side of the surface, and V_8N at the UN/V interface on the metal side. The remaining reactions are energetically blocked from forming, unless driven by entropy at finite temperatures or by irradiation, among which interactions at UN-W interfaces have the highest positive reaction energies, followed by interactions at UN-Mo interfaces.

The predicted defect formation energies provide a detailed understanding of phase transitions at the interfaces. At the interfaces of UN-V, UN-Nb, UN-Ta, and UN-Cr N-rich phases (≥ 50 at.%) are likely to reduce the N concentration and promote N incorporation in the metal, leading to the formation of more nitrides on the metal side (except for UVN_2 and $UTaN_2$). Whereas tungsten nitrides and molybdenum nitrides are in equilibrium with UN and the corresponding metal and no further reaction is initiated, leading to a stable and passive interface.

The inter-diffusion behaviors were studied by computing the diffusion coefficients with DFT calculations and SCMF theory. The diffusivity of V, Nb, Ta, Cr, Mo, and W in UN are predicted to be sig-

nificantly low. The flux coupling simulations demonstrate that these metal solutes are expected to be enriched next to the defect sinks (e.g. dislocation lines, grain boundaries, free surface, interfaces and so on) which prevents further contamination of the fuel by metals. The character of the diffusivity of N in the metals is critical, where N atoms diffuse faster in Cr, Mo, and W than in V, Nb, and Ta. However, in addition to the fact that the incorporation of N in W and Mo is energetically unfavorable, nitrogen impurities are unavailable because W and Mo metals are in equilibrium with UN.

To conclude, from the calculations here presented, Mo and W are the most promising candidates to provide a stable inhibition of the UN/UNO₂ reactions and to act as an efficient barrier for a composite fuel. Experimental verification has been performed and will be reported in subsequent publications. The analysis of those experiments remind us of the importance of oxygen in evaluating the performance of UN-X-UN fuel but a complete study of those reactions is deemed outside the scope of this work. The method-

ology described in this work will be applied to study the reactions at the UNO₂/metal interface and diffusion of O through metal in further work.

ACKNOWLEDGMENTS

Huan Liu is financially supported by the China Scholarship Council (No. 201700260222). Diogo R. Costa is financially supported by the Swedish Foundation for Strategic Research (SSF, Stiftelsen för Strategisk Forskning), under the project reference number ID17-0078. The computations were performed on resources provided by the Swedish National Infrastructure for Computing (SNIC) at PDC, KTH. This work contributes to the Joint Program on Nuclear Materials (JPNM) of the European Energy Research Alliance (EERA).

REFERENCES

-
- [1] P.E. Evans, T.J. Davies, Uranium nitrides, *J. Nucl. Mater.* 10 (1963) 43–55. [https://doi.org/10.1016/0022-3115\(63\)90115-6](https://doi.org/10.1016/0022-3115(63)90115-6).
 - [2] G.A. Rama Rao, S.K. Mukerjee, V.N. Vaidya, V. Venugopal, D.D. Sood, Oxidation and hydrolysis kinetic studies on UN, *J. Nucl. Mater.* 185 (1991) 231–241. [https://doi.org/10.1016/0022-3115\(91\)90340-D](https://doi.org/10.1016/0022-3115(91)90340-D).
 - [3] D.A. Lopes, S. Uygur, K. Johnson, Degradation of UN and UN-U₃Si₂ pellets in steam environment, *J. Nucl. Sci. Technol.* 54 (2017) 405–413. <http://doi.org/10.1080/00223131.2016.1274689>.
 - [4] M. Jolkkonen, P. Malkki, K. Johnson, J. Wallenius, Uranium nitride fuels in superheated steam, *J. Nucl. Sci. Technol.* 54 (2017) 513–519. <http://doi.org/10.1080/00223131.2017.1291372>.
 - [5] J.K. Watkins, D.P. Butt, B.J. Jaques, Microstructural degradation of UN and UN-UO₂ composites in hydrothermal oxidation conditions, *J. Nucl. Mater.* 518 (2019) 30–40. <https://doi.org/10.1016/j.jnucmat.2019.02.027>.
 - [6] P.A. Lessing, Oxidation protection of uranium nitride fuel using liquid phase sintering, INL/EXT-12-24974, technical report, 2012, INL. <http://doi.org/10.2172/1036778>.
 - [7] P. Malkki, The manufacturing of uranium nitride for possible use in light water reactors, Licentiate thesis, 2015, KTH Royal Institute of Technology, Stockholm, Sweden. <https://www.diva-portal.org/smash/get/diva2:816319/FULLTEXT01.pdf>.
 - [8] K.D. Johnson, A.M. Raftery, D.A. Lopes, J. Wallenius, Fabrication and microstructural analysis of UN-U₃Si₂ composites for accident tolerant fuel applications. *J. Nucl. Mater.* 477 (2016) 18–23. <https://doi.org/10.1016/j.jnucmat.2016.05.004>.
 - [9] L.H. Ortega, B.J. Blamer, J.A. Evans, S.M. McDevitt, Development of an accident tolerant fuel composite from uranium mononitride (UN) and uranium sesquisilicide (U₃Si₂) with increased uranium loading, *J. Nucl. Mater.* 471 (2016) 116–121. <https://doi.org/10.1016/j.jnucmat.2016.01.014>.
 - [10] B.J. Jaques, J. Watkins, J.R. Croteau, G.A. Alanko, B. Tyburska-Püschel, M. Meyer, P. Xu, E.J. Lahoda, D.P. Butt, Synthesis and sintering of UN-UO₂ fuel composites, *J. Nucl. Mater.* 466 (2015) 745–754. <https://doi.org/10.1016/j.jnucmat.2015.06.029>.
 - [11] J.H. Yang, D.-J. Kim, K.S. Kim, Y.-H. Koo, UN-UO₂ composites with enhanced uranium density and thermal conductivity, *J. Nucl. Mater.* 465 (2015) 509–515. <https://doi.org/10.1016/j.jnucmat.2015.06.039>.
 - [12] Y. Mishchenko, Composite UN-UO₂ fuels, Master thesis in Nuclear Energy Engineering, 2018, KTH Royal Institute of Technology, Stockholm, Sweden.
 - [13] D.R. Costa, M. Hedberg, S.C. Middleburgh, J. Wallenius, P. Olsson, D.A. Lopes, UN microspheres embedded in UNO₂ matrix: an innovative accident tolerant fuel, *J. Nucl. Mater.* 540 (2020) 152355.

- <https://doi.org/10.1016/j.jnucmat.2020.152355>.
- [14] A.F. Weinberg, L. Yang, Interdiffusion between uranium-bearing reactor fuels and refractory-metal thermionic emitters, *Adv. Energy Convers.* 3 (1963). [https://doi.org/10.1016/0365-1789\(63\)90080-8](https://doi.org/10.1016/0365-1789(63)90080-8).
- [15] J.J. Cadwell, Progress report on NASA cermet studies identification SNC-12, January 1964, No. HW-80847 United States, 1964, Hanford Atomic Products Operation. <https://doi.org/10.2172/10146731>
- [16] P.D. Takkunen, Fabrication of CerMets of Uranium Nitride and Tungsten or Molybdenum from Mixed Powders and from Coated Particles, NASA-TN-D-5136, 1969, Lewis Research Center.
- [17] G. Kresse, Efficient iterative schemes for ab initio total-energy calculations using a plane-wave basis set, *Phys. Rev. B.* 54 (1996) 11169-11186. <https://doi.org/10.1103/PhysRevB.54.11169>.
- [18] G. Kresse, J. Hafner, R.J. Needs, Optimized norm-conserving pseudopotentials, *J. Phys. Condens. Matter.* 4 (1992) 7451-7468. <https://doi.org/10.1088/0953-8984/4/36/018>.
- [19] G. Kresse, From ultrasoft pseudopotentials to the projector augmented-wave method, *Phys. Rev. B.* 59 (1999) 1758-1775. <https://doi.org/10.1103/PhysRevB.59.1758>.
- [20] G. Kresse, J. Furthmüller, Efficiency of ab-initio total energy calculations for metals and semiconductors using a plane-wave basis set, *Comput. Mater. Sci.* 6 (1996) 15-50. [https://doi.org/10.1016/0927-0256\(96\)00008-0](https://doi.org/10.1016/0927-0256(96)00008-0).
- [21] P.E. Blöchl, Projector augmented-wave method, *Phys. Rev. B.* 50 (1994) 17953-17979. <https://doi.org/10.1103/PhysRevB.50.17953>.
- [22] J.P. Perdew, K.A. Jackson, M.R. Pederson, D.J. Singh, C. Fiolhais, Atoms, molecules, solids, and surfaces: Applications of the generalized gradient approximation for exchange and correlation, *Phys. Rev. B.* 46 (1992) 6671-6687. <https://doi.org/10.1103/PhysRevB.46.6671>.
- [23] A.I. Liechtenstein, V.I. Anisimov, and J. Zaanen, Density-functional theory and strong interactions: Orbital ordering in Mott-Hubbard insulators, *Phys. Rev. B* 52, R5467(R). <https://doi.org/10.1103/PhysRevB.52.R5467>
- [24] A. Claisse, M. Klipfel, N. Lindbom, M. Freyss, P. Olsson, GGA+U study of uranium mononitride: A comparison of the U-ramping and occupation matrix schemes and incorporation energies of fission products, *J. Nucl. Mater.* 478 (2016) 119-124. <https://doi.org/10.1016/j.jnucmat.2016.06.007>
- [25] H.J. Monkhorst, J.D. Pack, Special points for Brillouin-zone integrations, *Phys. Rev. B* 13, 5188. <https://doi.org/10.1103/PhysRevB.13.5188>
- [26] A. Jain, S.P. Ong, G. Hautier, W. Chen, W.D. Richards, S. Dacek, S. Cholia, D. Gunter, D. Skinner, G. Ceder, K.A. Persson, The Materials Project: A materials genome approach to accelerating materials innovation, *APL Materials*, 2013, 1(1), 011002. <https://doi.org/10.1063/1.4812323>
- [27] P. Söderlind, First-principles phase stability, bonding, and electronic structure of actinide metals, *J. Electron Spectrosc. Relat. Phenom.* 194 (2014) 2-7. <https://doi.org/10.1016/j.elspec.2013.11.009>
- [28] A. Jain, G. Hautier, S. P. Ong, C. J. Moore, C. C. Fischer, K. A. Persson, and G. Ceder, Formation enthalpies by mixing GGA and GGA+U calculations, *Phys. Rev. B* 84, 045115. <https://doi.org/10.1103/PhysRevB.84.045115>
- [29] O. Kubaschewski, C. Alcock, and P. Spencer, *Materials Thermochemistry*, 6ed. Oxford: Pergamon Press, 1993.
- [30] M. Nastar, A mean field theory for diffusion in a dilute multi-component alloy: a new model for the effect of solutes on self-diffusion, *Philos. Mag.* 85 (2005) 3767-3794. <https://doi.org/10.1080/14786430500228390>.
- [31] T. Schuler, L. Messina, M. Nastar, KineCluE: A kinetic cluster expansion code to compute transport coefficients beyond the dilute limit, *Comput. Mater. Sci.* 172 (2020). <https://doi.org/10.1016/j.commatsci.2019.109191>.
- [32] L. Messina, T. Schuler, M. Nastar, M.C. Marinica, P. Olsson, Solute diffusion by self-interstitial defects and radiation-induced segregation in ferritic Fe-X (X=Cr, Cu, Mn, Ni, P, Si) dilute alloys, *Acta Mater.* 191 (2020) 166-185. <https://doi.org/10.1016/j.actamat.2020.03.038>.
- [33] G. Henkelman, B.P. Uberuaga, H. Jónsson, Climbing image nudged elastic band method for finding saddle points and minimum energy paths, *J. Chem. Phys.* 113 (2000) 9901-9904. <https://doi.org/10.1063/1.1329672>.
- [34] H. Jónsson, G. Mills, K.W. Jacobsen, Nudged elastic band method for finding minimum energy paths of transitions, *Class. Quantum Dyn. Condens. Phase Simulations*, WORLD SCIENTIFIC (1998) 385-404.
- [35] G.H. Vineyard, Frequency factors and isotope effects in solid state rate processes, *J. Phys. Chem. Solids* 3 (1957) 121-127. [https://doi.org/10.1016/0022-3697\(57\)90059-8](https://doi.org/10.1016/0022-3697(57)90059-8)
- [36] K.H. Weyrich, Frozen phonon calculations: Lattice dynamics and Instabilities, *Ferroelectrics* 104 (1990) 183-194. <https://doi.org/10.1080/00150199008223822>
- [37] A. Togo, I. Tanaka, First principles phonon calculations in materials science, *Scripta Mater.* 108 (2015) 1-5. <https://doi.org/10.1016/j.scriptamat.2015.07.021>
- [38] K. D. Johnson, D. A. Lopes, Grain growth in uranium nitride prepared by spark plasma sintering, *J. Nucl. Mater.* 503 (2018) 75-80. <https://doi.org/10.1016/j.jnucmat.2018.02.041>

- [39] M.J. Klein, Diffusion Coefficient of Nitrogen in Chromium, *J. Appl. Phys.* 38 (1967) 167-170. <https://doi.org/10.1063/1.1708947>
- [40] R.W. Powers, M.V. Doyle, Diffusion of interstitial solutes in the group V transition metals, *J. Appl. Phys.* 30 (1959) 514-524. <https://doi.org/10.1063/1.1702398>
- [41] R.L. Wagner, Nitrogen diffusion and solubility in tungsten, *Metall. Trans.* 1 (1970) 3365-3370. <https://doi:10.1007/BF03037865>.
- [42] D.E. Weaver, Diffusivity and solubility of nitrogen in molybdenum and the trapping of nitrogen by carbon in molybdenum (No. UCRL-51182), october 1972, California Univ.
- [43] A. Anttila, and J. Hirvonen, Annealing behavior of nitrogen-implanted proton-irradiated molybdenum, *Appl. Phys. Lett.* 33 (1978) 394. <https://doi.org/10.1063/1.90388>

APPENDIX

TABLE A1. Formation enthalpies, ΔH_f , in eV/atom, of U-X-N binary and ternary compounds, where X= V, Nb, Ta, Cr, Mo, or W, compared to experimental results. The most stable phase of each case is shown in bold.

Phase	Space group	Calculated ΔH_f	Experimental ΔH_f [29]	Difference (calc. - exp.)	Calculation method
UN	Fm-3m	-1.57	-1.53	-0.04	GGA+U
V ₈ N	P42/mnm	-0.33			GGA
V ₂ N	P-31m	-0.98	-0.91	-0.06	GGA
VN	P-6m2	-1.17	-1.13	-0.04	GGA
UVN₂	Pnma	-1.43			GGA+U
V ₂ N ₃	P-3m1	-0.77			GGA
Nb ₂ N	P-31m	-0.88	-0.87	-0.02	GGA
NbN	P-6m2	-1.08	-1.22	0.14	GGA
UNbN ₂	Pnma	-1.40			GGA+U
Nb ₅ N ₆	P63/mcm	-1.02			GGA
Ta ₂ N	P-31m	-0.92	-0.94	0.02	GGA
TaN	P-62m	-1.18	-1.31	0.13	GGA
UTaN₂	Pnma	-1.83			GGA+U
Ta ₅ N ₆	P63/mcm	-1.14			GGA
Ta ₃ N ₅	Cmcm	-1.06			GGA
Cr ₂ N	P-31m	-0.42	-0.43	0.02	GGA
Cr ₃ N ₂	R-3c	-0.44			GGA
CrN	P-6m2	-0.54	-0.61	0.06	GGA
U₂CrN₃	Immm	-1.34			GGA+U
Cr ₃ N ₄	P63/m	-0.34			GGA
Mo ₂ N	I41/amd	-0.32	-0.28	-0.04	GGA
MoN	P63mc	-0.46			GGA
Mo _{1.5} N _{1.6}	Cc	-0.45			GGA
Mo ₂ N ₃	P-1	-0.18			GGA
WN	P-6m2	-0.10			GGA
W₂N₃	Cm	-0.48			GGA
WN ₂	P-6m2	-0.30			GGA

TABLE A2. UN/X (X= V, Nb, Ta, Cr, Mo, or W) reaction energies, ΔH_r , listed in increasing molar fraction, x , of UN in the reaction: $x\text{UN} + (1-x)\text{X}$. The reactions in bold represent the minimum ΔH_r , i.e., on the reaction energy convex hull.

Metal	x	Reaction	ΔH_r (eV/atom)
V	1/9	UN+8V=V₈N+U	0.01
	1/3	UN+2V=V ₂ N+U	0.05
	1/2	UN+V=VN+U	0.27
	3/5	3UN+2V=V ₂ N ₃ +3U	0.70
	2/3	2UN+V=UVN ₂ +U	0.11
	Nb	1/3	UN+2Nb=Nb ₂ N+U
1/2		UN+Nb=NbN+U	0.33
5/9		6UN+5Nb=Nb ₅ N ₆ +6U	0.45
2/3		2UN+Nb=UNbN₂+U	0.11
Ta		1/3	UN+2Ta=Ta ₂ N+U
	1/2	UN+Ta=TaN+U	0.26
	5/9	6UN+5Ta=Ta ₅ N ₆ +2U	0.37
	5/8	5UN+3Ta=Ta ₃ N ₅ +5U	0.55
	2/3	2UN+Ta=UTaN₂+U	-0.21
Cr	1/3	UN+2Cr=Cr ₂ N+U	0.47
	2/5	2UN+3Cr=Cr ₃ N ₂ +2U	0.56
	1/2	UN+Cr=CrN+U	0.68
	4/7	4UN+3Cr=Cr ₃ N ₄ +4U	0.78
	3/4	3UN+Cr=U₂CrN₃+U	0.20
Mo	1/3	UN+2Mo=Mo₂N+U	0.55
	1/2	UN+Mo=MoN+U	0.74
	1/2	16UN+15Mo=Mo ₁₅ N ₁₆ +16U	0.92
	3/5	3UN+2Mo=Mo ₂ N ₃ +3U	1.07
W	1/2	UN+W=WN+U	0.98
	3/5	3UN+2W=W₂N₃+U	0.88
	2/3	2UN+W=WN ₂ +2U	1.08